Journal of Thermal Analysis and Calorimetry (2019) 135:3171–3179
https://doi.org/10.1007/s10973-018-7530-2

# Thermodynamic and thermal energy storage properties of a new medium-temperature phase change material

Ju-Lan Zeng[1] · Li Shu[1] · Liu-Mo Jiang[1] · Yu-Hang Chen[1] · Yu-Xiang Zhang[1] · Ting Xie[1] · Li-Xian Sun[2] · Zhong Cao[1]

Received: 12 February 2018 / Accepted: 3 July 2018 / Published online: 13 July 2018


**Abstract**
Phase change materials (PCMs) that can store the heat energy obtained from intermittent solar irradiation are very important for solar energy absorption cooling system. In this work, an organic compound that melts at the temperature of 368.2 ± 0.5 K was applied as PCM. The specific heat capacities of the PCM were measured by temperature-modulated differential scanning calorimetry from 198.15 to 431.15 K. The thermodynamic functions of $[H_T–H_{298.15}]$ and $[S_T–S_{298.15}]$ were then calculated based on the measured heat capacities data. Afterward, the long-term cyclic thermal energy storage stability and thermal stability of the PCM were investigated. The results show that the PCM melted and crystallized at about 368 and 364 K, respectively, with a phase change enthalpy ($\Delta_{trans}H$) of 21 kJ mol$^{-1}$ (130 J g$^{-1}$). Additionally, it exhibited good long-term cyclic thermal energy storage stability and thermal stability. Hence, the PCM could be applied as good PCM for solar energy absorption cooling.

**Keywords** Phase change materials · Solar absorption cooling · Thermal energy storage · Thermodynamic properties

## Introduction

Solar energy absorption cooling has drawn more and more attention because it could directly transfer the "hot" solar energy to "cool" energy [1, 2]. It is especially beneficial for indoor temperature controlling and environmental protection in hot climate region, as it could save great amounts of energy by exploiting the inexhaustible solar energy [3]. Normally, the supply of solar irradiation varies daily and seasonally. Hence, a thermal energy storage system is indispensable for solar energy absorption cooling system, as it can store the thermal energy which is obtained from solar irradiation, and then, the stored thermal energy can be applied to power the absorption chiller [4]. Phase change materials (PCMs) are one of the best thermal energy storage materials because it can absorb or release large amounts of thermal energy in a small temperature range [5–9]. It was reported that the coefficient of performance (COP) of the absorption chiller can be improved by PCMs [10]. Hence, latent heat thermal storage (LHTS) unit incorporated with PCMs is particularly attractive for solar energy absorption cooling system [11].

The heat source inlet temperature for the absorption chiller of a solar energy absorption cooling system (LiBr/$H_2O$ absorption system) should be in the range of 363–393 K [12]. It was reported that the best COP for a single-effect absorption cooling system was obtained when the inlet temperature was in the range of 353–373 K [1]. Besides, Vasilescu et al. [13] have proposed that the inlet temperature of double-effect system should be higher than 413 K. The phase change temperature of the selected PCMs for solar energy absorption cooling system should be at least 10 K higher than the above-mentioned temperature

✉ Ju-Lan Zeng
julan_zeng@163.com

[1] Collaborative Innovation Center of Micro/nano Bio-sensing and Food Safety Inspection, Hunan Provincial Key Laboratory of Materials Protection for Electric Power and Transportation, School of Chemistry and Biological Engineering, Changsha University of Science and Technology, Changsha 410114, People's Republic of China

[2] Guangxi Key Laboratory of Information Materials, Guangxi Collaborative Innovation Center of Structure and Property for New Energy and Materials, Department of Material Science and Engineering, Guilin University of Electrical Technology, Guilin 541004, People's Republic of China

when the temperature gradient between the PCMs and the heat transfer fluid is concerned [14]. That is, the phase change temperature of a PCM candidate should be higher than 363 K for single-effect system and higher than 423 K for double-effect system, respectively.

Unfortunately, PCMs that crystallize (release the stored thermal energy) at the above-mentioned temperature range are limited. A very recent review has collected almost all possible PCMs for solar energy absorption cooling system [15]. However, lots of them have certain drawbacks. Inorganic hydrated salts PCMs [16, 17] that melted at the above-mentioned temperature range should be excluded due to that the temperature is close to or higher than the boiling point of water, resulting in a rapid dehydration of the PCMs over melting–crystallizing cycles. Some salts or salts mixtures can melt and freeze at this temperature range [18, 19], but they are highly corrosive. Some sugar alcohols also have the corresponding phase change temperature [20, 21]. Unfortunately, they exhibit ultra-high supercooling [7, 22, 23]. Brancato et al. investigated the thermal energy storage properties of three kinds of commercial PCMs and six kinds of neat chemical compounds. They found that, although all the neat chemical compounds exhibit high phase change enthalpy ($\Delta_{trans}H$), they are not stable, showing high supercooling, allotropic phase transition, incongruent melting or even absence of recrystallization [14]. Hence, it is desperately needed to find new PCMs that can store and release thermal energy in the above-mentioned temperature range and possess stable phase change thermal energy storage properties.

In response to this demand, an organic compound, namely (*E*)-3-phenylbut-2-enoic acid, that melts at the temperature range of 368.2 ± 0.5 K was presented in this work. The compound has been applied as a substrate in catalyzed organic synthesis chemistry. Here, it is viewed as PCM candidate that can be applied in solar energy absorption cooling system. Its thermal energy storage property, preliminary long-term cyclic thermal energy storage stability, as well as thermal stability were investigated. Here, the cost of the materials was not considered because it is believed that upon large-scale bulk production on the worldwide market, materials are likely to obtain a reasonable price.

Additionally, it is generally accepted that thermodynamic properties are one of the most important properties of a substance [24], and specific heat capacity is the most fundamental thermodynamic property. From the specific heat capacity, other thermodynamic properties, such as enthalpy and entropy, can be obtained. Furthermore, heat capacity is also required to model the effectiveness of the PCM and to optimize the quantity needed within the space [9, 25]. Temperature-modulated differential scanning calorimetry (TMDSC) is an accurate and easy method to measure the specific heat capacity of a substance [26, 27]. In this work, the specific heat capacities of the PCM were measured by TMDSC and then the thermodynamic parameters such as entropy and enthalpy were calculated.

## Experimental

### Materials

The PCM ((*E*)-3-phenylbut-2-enoic acid) with the purity higher than 98% was obtained commercially and used without further purification. The molecular structure of the PCM is shown in Fig. 1.

### Characterization

The thermal energy storage properties of the samples were measured by differential scanning calorimetry (DSC, TA, Q2000) coupled with a refrigerating cooling system 90 (RCS 90, TA) under a constant flow of dry nitrogen with the flow rate of 50 mL $min^{-1}$. The heating rate of the DSC experiments was 10 K $min^{-1}$. The preliminary long-term cyclic thermal energy storage stability of the samples was investigated by cyclic DSC experiments over 50 cycles under the same experimental condition. The low temperature of the cyclic DSC experiments was 303.15 K, while the high temperature was 393.15 K. After a heating or cooling run was completed, the sample stayed in isothermal state at the high or low temperature for 3 min before the next heating or cooling run was started, and the heating/cooling rate was 10 K $min^{-1}$. All DSC experiments were repeated for three times using different samples, and the mean values are reported. Prior to the DSC experiments, the instrument was calibrated using indium (99.999%) as the standard material. The uncertainties of the DSC system are typically ± 5% for phase change enthalpy ($\Delta_{trans}H$) and ± 0.5 K for temperature. The thermal stability of the samples was characterized by means of thermogravimetry (TG)/differential thermal analysis (DTA) on a thermogravimetric analyzer (NETZSCH STA 409 PG/PC) from room temperature (298 K) to 773 K with the heating rate of 10 K $min^{-1}$ using $N_2$ as carrier gas. The

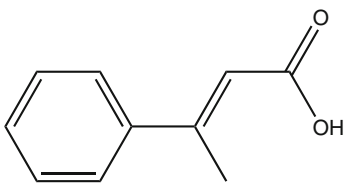


(*E*)-3-phenylbut-2-enoic acid

**Fig. 1** Molecular structure of the PCM

analyzer was calibrated using $CaC_2O_4{\cdot}H_2O$ (99.9%) prior to the experiment. The thermal conductivity of the samples at room temperature was measured by means of the steady-state heat flow method using a thermal conductivity tester (DRX-II-RW, Xiangtan Huafeng Instrument Manufacturing Co., Ltd, China). The PCM was melted in a mold with a diameter of 10 mm and then cooled to obtain cylinders. Solid disks of the PCM with the height of about 2–3 mm were then obtained from the bottom of the cylinders to avoid possible pores. The hot plate of the tester was set at 308 K, and the cold plate was cooled by 288 K water. A PCM disk was mounted between the two plates. The thermal conductivity of the disk was measured when the temperature of the two plates remained stable for more than 1 h. The uncertainty of the tester was less than 15%.

### Heat capacities measurement

Heat capacities measurements were taken on a differential scanning calorimeter (Q1000, TA) coupled with a RCS 90 using high-purity (99.999%) nitrogen as purge gas (50 mL $min^{-1}$). The temperature (± 0.5 K) and energy scale (± 5%) of the instrument were initially calibrated with indium (99.999%) as the standard material in the standard DSC mode. The heat capacity calibration was performed by using a standard sapphire ($\alpha$-$Al_2O_3$) as a standard material over the temperature range of 183.15–483.15 K. The calibration was performed according to our previously reported procedure [28]. Based on measurements of a reference material (benzoic acid) with known $C_p$, the overall uncertainty in the heat capacity is less than 5%. For sample measurements, the procedure was similar to that of the calibration except the temperature of equilibration was 193.15 K and the terminal heating temperature was 433.15 K. Samples were crimped in non-hermetic aluminum pans with lids. Sample mass was weighed on a Mettler Toledo electrobalance (AB135-S, Classic) with an accuracy of ± 0.01 mg.

## Results and discussion

### DSC characterization of the PCM

The heating DSC curve of the PCM is depicted in Fig. 2. The figure shows clearly that upon heating, the PCM exhibited a single and sharp endothermic peak corresponding to the melting process. The onset melting temperature ($T_{on,m}$) and the melting phase change enthalpy ($\Delta_m H$) of the PCM are also shown in Fig. 2. The $T_{on,m}$ of the PCM was 368.2 ± 0.5 K and the $\Delta_m H$ was 129.5 ± 6.5 J $g^{-1}$ (21.0 ± 1.05 kJ $mol^{-1}$). The $\Delta_m H$ of the PCM is close to some polyethylene glycols (PEG) with

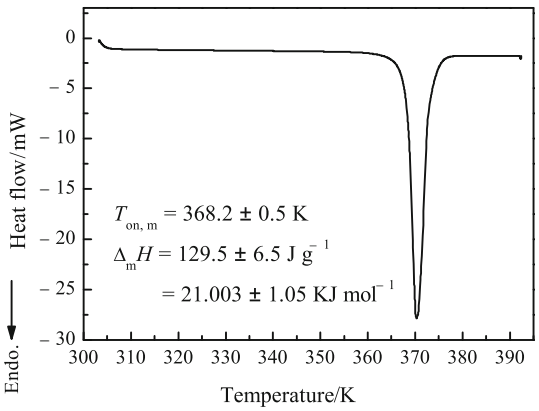


**Fig. 2** Heating DSC curve of the PCM

medium molecular wight such as PEG 8000 (∼ 148 J $g^{-1}$, [29]) and PEG 2000 (∼ 141 J $g^{-1}$, [30]) and is higher than that of polyethylene glycols (PEG) with lower molecular wight [16, 30] and some other potential PCMs such as biphenyl and naphthalene/benzoic acid mixtures [16]. The suitable melting temperature and the relatively large $\Delta_m H$ of the PCM implied that it is a good PCM candidate to be applied as thermal energy storage material in solar absorption cooling system.

### Heat capacities of the PCM

The specific heat capacities data over the temperature range of 198.15–431.15 K of the PCM obtained from three duplicated experiments are given in Table 1. The experimental standard deviation is also presented. Low experimental standard deviations were obtained and show reasonably good reproducibility over the experimental temperature range. The experimental specific molar heat capacities of the PCM are shown in Fig. 3. It can be seen that only one thermal anomaly, which was caused by the melting of the PCM, existed on the curve. The curve can be divided into three regions: solid state before the thermal anomaly; liquid state after the thermal anomaly and phase transition region corresponding to the thermal anomaly. The PCM was in solid state when the temperature was lower than 363.15 K and was in liquid state when the temperature was higher than 378.15 K. In both solid and liquid states, the specific heat capacities of the PCM increased monotonically in a smooth and continuous manner. In general, particles in common materials move more vigorously at higher temperature than at lower temperature. Hence, for a certain amount of specific materials at higher temperature, more energy is needed to increase a same temperature than at lower temperature, thus resulting in the increase in specific heat capacities when the temperature is increased. The monotones increase in the specific heat capacities of the PCM in a smooth and

**Table 1** The data of three reduplicate TMDSC experiments for the PCM

| *T*/K | $C_p$ (exp)/J K$^{-1}$ g$^{-1}$ | | | | Standard deviation |
|---|---|---|---|---|---|
| | 1 | 2 | 3 | Average | |
| 198.15 | 0.7376 | 0.6575 | 0.6443 | 0.6798 | 0.0505 |
| 203.15 | 0.7691 | 0.6930 | 0.6804 | 0.7141 | 0.0480 |
| 208.15 | 0.7938 | 0.7211 | 0.7094 | 0.7414 | 0.0457 |
| 213.15 | 0.8172 | 0.7456 | 0.7350 | 0.7660 | 0.0447 |
| 218.15 | 0.8400 | 0.7708 | 0.7594 | 0.7901 | 0.0436 |
| 223.15 | 0.8726 | 0.8074 | 0.7886 | 0.8229 | 0.0441 |
| 228.15 | 0.8952 | 0.8317 | 0.8140 | 0.8470 | 0.0427 |
| 233.15 | 0.9092 | 0.8445 | 0.8297 | 0.8611 | 0.0423 |
| 238.15 | 0.9253 | 0.8584 | 0.8481 | 0.8773 | 0.0419 |
| 243.15 | 0.9444 | 0.8776 | 0.8666 | 0.8962 | 0.0421 |
| 248.15 | 0.9650 | 0.8976 | 0.8871 | 0.9166 | 0.0423 |
| 253.15 | 0.9841 | 0.9192 | 0.9080 | 0.9371 | 0.0411 |
| 258.15 | 1.0053 | 0.9395 | 0.9294 | 0.9580 | 0.0412 |
| 263.15 | 1.0250 | 0.9598 | 0.9498 | 0.9782 | 0.0409 |
| 268.15 | 1.0450 | 0.9811 | 0.9730 | 0.9997 | 0.0395 |
| 273.15 | 1.0649 | 1.0014 | 0.9935 | 1.0200 | 0.0391 |
| 278.15 | 1.0844 | 1.0232 | 1.0149 | 1.0408 | 0.0379 |
| 283.15 | 1.1057 | 1.0426 | 1.0348 | 1.0610 | 0.0389 |
| 288.15 | 1.1249 | 1.0638 | 1.0560 | 1.0816 | 0.0377 |
| 293.15 | 1.1444 | 1.0829 | 1.0752 | 1.1008 | 0.0379 |
| 298.15 | 1.1642 | 1.1028 | 1.0950 | 1.1207 | 0.0379 |
| 303.15 | 1.1838 | 1.1209 | 1.1156 | 1.1401 | 0.0380 |
| 308.15 | 1.2032 | 1.1402 | 1.1347 | 1.1594 | 0.0381 |
| 313.15 | 1.2221 | 1.1604 | 1.1552 | 1.1792 | 0.0372 |
| 318.15 | 1.2421 | 1.1920 | 1.1848 | 1.2063 | 0.0312 |
| 323.15 | 1.2645 | 1.2228 | 1.2178 | 1.2350 | 0.0257 |
| 328.15 | 1.2878 | 1.2600 | 1.2666 | 1.2715 | 0.0146 |
| 333.15 | 1.3125 | 1.3249 | 1.3457 | 1.3277 | 0.0168 |
| 338.15 | 1.3534 | 1.3546 | 1.3999 | 1.3693 | 0.0265 |
| 343.15 | 1.3883 | 1.3765 | 1.4291 | 1.3980 | 0.0276 |
| 348.15 | 1.4083 | 1.3856 | 1.4408 | 1.4116 | 0.0277 |
| 353.15 | 1.4357 | 1.4115 | 1.4665 | 1.4379 | 0.0276 |
| 358.15 | 1.4665 | 1.4299 | 1.4847 | 1.4604 | 0.0279 |
| 363.15 | 1.5157 | 1.4714 | 1.5279 | 1.5050 | 0.0298 |
| 368.15 | Phase change region | | | | |
| 373.15 | | | | | |
| 378.15 | 2.2077 | 2.1093 | 2.1221 | 2.1463 | 0.0535 |
| 383.15 | 2.2859 | 2.1742 | 2.1905 | 2.2169 | 0.0603 |
| 388.15 | 2.4418 | 2.3199 | 2.3174 | 2.3597 | 0.0711 |
| 393.15 | 2.6564 | 2.5173 | 2.4933 | 2.5557 | 0.0881 |
| 398.15 | 2.9508 | 2.7790 | 2.7244 | 2.8181 | 0.1181 |
| 403.15 | 3.3743 | 3.1276 | 3.0415 | 3.1811 | 0.1727 |
| 408.15 | 3.8780 | 3.5935 | 3.4259 | 3.6325 | 0.2286 |
| 413.15 | 4.2103 | 4.0483 | 3.8097 | 4.0228 | 0.2015 |
| 418.15 | 4.4818 | 4.3733 | 4.2520 | 4.3690 | 0.1150 |
| 423.15 | 4.7757 | 4.7306 | 4.9479 | 4.8181 | 0.1147 |
| 428.15 | 4.5964 | 4.6007 | 5.6776 | 4.9583 | 0.6230 |
| 431.15 | 5.1238 | 4.9403 | 5.8400 | 5.3014 | 0.4754 |

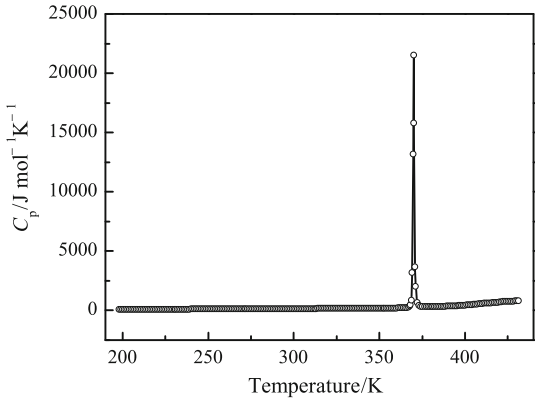


**Fig. 3** $C_{p,\,m}$ of the PCM from 198.15 to 431.15 K (mean values of three duplicated experiments; the uncertainties are ± 0.5 K for *T* and ± 5% for $C_p$)

continuous manner also indicated that they are stable in the corresponding temperature range.

The specific heat capacities of the PCM were fitted to polynomial equations by means of nonlinear least square fitting.

For the solid phase over the temperature range of 198.15–363.15 K:

$$C_{p,m}(s) = 169.131 + 50.296X + 17.948X^2 + 34.331X^3 - 10.018X^4 - 19.6X^5, \quad (1)$$

where

$$X = (T - (T_{max} + T_{min})/2)/((T_{max} - T_{min})/2) \quad (2)$$

is the reduced temperature, in which *T* is the experimental temperature and $T_{max}$ is the upper limit (363.15 K), while $T_{min}$ is the lower limit (198.15 K) of the above temperature region. With a reduced temperature, the absolute temperature is normalized such that all experimental data extend from −1 to 1 for both solid and liquid data sets, and therefore, it can present a more accurate curve fitting [31]. The correlation coefficient of the fitting is $R^2 = 0.9985$.

For the liquid phase over the temperature range of 378.15–431.15 K:

$$C_{p,m}(l) = 537.44 + 348.42X + 82.777X^2 - 156.72X^3 - 23.654X^4 + 60.788X^5, \quad (3)$$

where $X$ is obtained according to Eq. (2) with $T_{max}$ = 431.15 K and $T_{min}$ = 378.15 K. The correlation coefficient of the fitting is $R^2$ = 0.9986. The data of experimental and simulated molar heat capacities are listed in Table 2.

The $C_{p,\,m}$ of some PCMs candidates, such as 1-naphthol [32], sorbitol [33] and xylitol [34], that melt over the temperature range of 363–373 K was reported in references. The $C_{p,\,m}$ of the PCM reported in this work is close to that of 1-naphthol but is lower than that of sorbitol and xylitol. Both the PCM and 1-naphthol have ten carbon atoms in a molecule. Besides, the PCM has a carboxyl group, while 1-naphthol has a hydroxyl group in a molecule, which means that the hydrogen bonds in the PCM would be a little bit stronger than in 1-naphthol. As a result, the $C_{p,\,m}$ of the PCM is higher than of 1-naphthol, but the specific mass heat capacities of the PCM are lower than those of 1-naphthol due to that the molecular weight of the PCM is higher than 1-naphthol. On the other hand, there are a lot of hydroxyl groups in xylitol and sorbitol, resulting in a lot of hydrogen bonds in their crystals, and thus xylitol and sorbitol possess higher $C_{p,\,m}$ and specific mass heat capacities than the PCM.

## Thermodynamic properties of the PCM

The $\Delta_m H$ of the PCM can be obtained by integrating the $C_p$–$T$ curve from the starting temperature to the terminating temperature over the corresponding phase transition region, while the melting entropy ($\Delta_m S$) can be derived according to the following equation [35]:

$$\Delta_m S = {}^{\Delta_m H}/_{T_{on,m}}, \tag{4}$$

where $T_{on,m}$ is the onset temperature of the heat capacity curve. The values of the $T_{on,m}$ and the $\Delta H_m$ of the PCM were determined to be 369.2 ± 0.5 K and 19.99 ± 1.0 kJ mol$^{-1}$, respectively, which are agreed well with the results of DSC experiment, and the $\Delta S_m$ is 53.59 ± 2.7 J mol$^{-1}$ K$^{-1}$.

Enthalpy and entropy are important basic thermodynamic functions for any substances. Based on the heat capacities polynomials and the thermodynamic relationships, the $[H_T–H_{298.15}]$ and $[S_T–S_{298.15}]$ of the PCM were calculated over the experimental temperature range with an interval of 5 K related to 298.15 K. The thermodynamic relationships are as follows:

Before melting:

$$H_T - H_{298.15} = \int_{298.15}^{T} C_{p,m}(s)\mathrm{d}T, \tag{5}$$

**Table 2** The experimental and fitted molar heat capacities of the PCM

| $T$/K | $C_{p,m}$ (exp)/J mol$^{-1}$ K$^{-1}$ | $C_{p,m}$ (fit)/J mol$^{-1}$ K$^{-1}$ | RD% |
|---|---|---|---|
| 198.15 | 110.2542 | 112.0323 | 1.59 |
| 203.15 | 115.8208 | 115.7952 | − 0.02 |
| 208.15 | 120.2492 | 119.7884 | − 0.38 |
| 213.15 | 124.2269 | 123.8874 | − 0.27 |
| 218.15 | 128.1362 | 127.9944 | − 0.11 |
| 223.15 | 133.4559 | 132.0333 | − 1.08 |
| 228.15 | 137.3644 | 135.9531 | − 1.04 |
| 233.15 | 139.6623 | 139.7160 | 0.04 |
| 238.15 | 142.2840 | 143.3046 | 0.71 |
| 243.15 | 145.3502 | 146.7159 | 0.93 |
| 248.15 | 148.6514 | 149.9425 | 0.86 |
| 253.15 | 151.9839 | 153.0411 | 0.69 |
| 258.15 | 155.3803 | 156.0239 | 0.41 |
| 263.15 | 158.6528 | 158.9291 | 0.17 |
| 268.15 | 162.1395 | 161.8000 | − 0.21 |
| 273.15 | 165.4226 | 164.6830 | − 0.45 |
| 278.15 | 168.8059 | 167.6263 | − 0.70 |
| 283.15 | 172.0849 | 170.6784 | − 0.82 |
| 288.15 | 175.4162 | 173.8847 | − 0.88 |
| 293.15 | 178.5339 | 177.2866 | − 0.70 |
| 298.15 | 181.7570 | 180.9195 | − 0.46 |
| 303.15 | 184.9066 | 184.8109 | − 0.05 |
| 308.15 | 188.0304 | 188.9773 | 0.50 |
| 313.15 | 191.2545 | 193.3992 | 1.11 |
| 318.15 | 195.6454 | 198.1166 | 1.25 |
| 323.15 | 200.3050 | 203.0544 | 1.35 |
| 328.15 | 206.2120 | 208.2245 | 0.97 |
| 333.15 | 215.3288 | 213.5390 | − 0.84 |
| 338.15 | 222.0754 | 218.9157 | − 1.44 |
| 343.15 | 226.7342 | 224.2501 | − 1.11 |
| 348.15 | 228.9368 | 229.4082 | 0.21 |
| 353.15 | 233.2089 | 234.2295 | 0.44 |
| 358.15 | 236.8541 | 238.5269 | 0.70 |
| 363.15 | 244.0892 | 242.0793 | − 0.83 |
| 368.15 | Phase change region | | |
| 373.15 | | | |
| 378.15 | 348.1045 | 344.0806 | − 1.17 |
| 383.15 | 359.5477 | 361.3300 | 0.49 |
| 388.15 | 382.7052 | 381.1818 | − 0.40 |
| 393.15 | 414.4924 | 412.8658 | − 0.39 |
| 398.15 | 457.0481 | 459.1361 | 0.45 |
| 403.15 | 515.9271 | 518.0154 | 0.40 |
| 408.15 | 589.1337 | 584.5394 | − 0.79 |
| 413.15 | 652.4334 | 652.5011 | 0.01 |
| 418.15 | 708.5916 | 716.1949 | 1.06 |
| 423.15 | 781.4197 | 772.1612 | − 1.20 |
| 428.15 | 804.1561 | 820.9302 | 2.04 |
| 431.15 | 859.8017 | 849.0524 | − 1.27 |

$$S_T - S_{298.15} = \int_{298.15}^{T} \frac{C_{p,m}(s)}{T} dT, \quad (6)$$

After melting:

$$H_T - H_{298.15} = \int_{298.15}^{T_{on,m}} C_{p,m}(S)dT + \Delta_m H + \int_{T_f}^{T} C_{p,m}(l)dT, \quad (7)$$

$$S_T - S_{298.15} = \int_{298.15}^{T_{on,m}} \frac{C_{p,m}(s)}{T} dT + \Delta_m S + \int_{T_f}^{T} \frac{C_{p,m}(l)}{T} dT, \quad (8)$$

where $T_{on,m}$ is the onset temperature of the heat capacity curve, while $T_f$ is the temperature at which the melting ended. The calculated thermodynamic functions [$H_T$–$H_{298.15}$] and [$S_T$–$S_{298.15}$] of the PCM are given in Table 3.

From the calculated [$H_T$–$H_{298.15}$], an energy storage curve of the PCM over the temperature range from 298.15 to 431.15 K could be obtained and is depicted in Fig. 4. In the solid and liquid states, the PCMs store thermal energy due to the heat capacity. In the phase change region, the energy storage curve shows a jump, indicating that a lot of thermal energy could be stored or released by phase change in the PCM.

## Long-term cyclic thermal energy storage and release stability of the PCM

Preliminary investigation of the long-term cyclic thermal energy storage/release stability of the PCM was carried out by means of 50 cyclic DSC experiments. The cyclic DSC experiment was repeated for three times using different samples, and the results show good reproducibility. Selected cyclic heating and cooling DSC curves of the PCM are shown in Fig. 5. The figure shows that there was only one endothermic/exothermic peak exhibited on all the heating/cooling curves and the shape of the endo/exothermic peaks was similar. The single and similar endo/exothermic peak implied that the PCM underwent a one-step melting/crystallizing procedure when it was heated/cooled over all cycles, which is favor for it to be applied as PCM. The $T_{on,m}$, the peak crystallizing temperature ($T_{p,cr}$), the $\Delta_m H$ and the crystallizing phase change enthalpy ($\Delta_{cr} H$) of the PCM during the 50 cycles are depicted in Fig. 5. Because we could not obtain the onset crystallizing temperature ($T_{on,cr}$) of some cooling runs due to supercooling and the principle of the DSC instrument [23], here we choose the $T_{p,cr}$ rather than the $T_{on,cr}$ to evaluate the freezing temperature. Figure 6 shows that the

**Table 3** Calculated thermodynamic function data of the PCM

| $T$/K | $H_T$–$H_{298.15}$/KJ mol$^{-1}$ | $S_T$–$S_{298.15}$/J mol$^{-1}$ K$^{-1}$ |
|---|---|---|
| 198.15 | − 14.83 | − 59.64 |
| 203.15 | − 14.26 | − 56.80 |
| 208.15 | − 13.67 | − 53.94 |
| 213.15 | − 13.06 | − 51.05 |
| 218.15 | − 12.43 | − 48.13 |
| 223.15 | − 11.78 | − 45.18 |
| 228.15 | − 11.11 | − 42.21 |
| 233.15 | − 10.42 | − 39.23 |
| 238.15 | − 9.71 | − 36.22 |
| 243.15 | − 8.99 | − 33.21 |
| 248.15 | − 8.25 | − 30.19 |
| 253.15 | − 7.49 | − 27.17 |
| 258.15 | − 6.72 | − 24.15 |
| 263.15 | − 5.93 | − 21.12 |
| 268.15 | − 5.13 | − 18.11 |
| 273.15 | − 4.31 | − 15.09 |
| 278.15 | − 3.48 | − 12.08 |
| 283.15 | − 2.63 | − 9.06 |
| 288.15 | − 1.77 | − 6.05 |
| 293.15 | − 0.90 | − 3.03 |
| 298.15 | 0.00 | 0.00 |
| 303.15 | 0.91 | 3.04 |
| 308.15 | 1.85 | 6.10 |
| 313.15 | 2.80 | 9.17 |
| 318.15 | 3.78 | 12.27 |
| 323.15 | 4.79 | 15.40 |
| 328.15 | 5.81 | 18.56 |
| 333.15 | 6.87 | 21.75 |
| 338.15 | 7.95 | 24.97 |
| 343.15 | 9.06 | 28.22 |
| 348.15 | 10.19 | 31.50 |
| 353.15 | 11.35 | 34.81 |
| 358.15 | 12.53 | 38.13 |
| 363.15 | 13.74 | 41.47 |
| 368.15 | Phase change region | |
| 373.15 | | |
| 378.15 | 36.30 | 102.50 |
| 383.15 | 38.07 | 107.14 |
| 388.15 | 39.92 | 111.94 |
| 393.15 | 41.90 | 117.01 |
| 398.15 | 44.08 | 122.50 |
| 403.15 | 46.51 | 128.59 |
| 408.15 | 49.27 | 135.38 |
| 413.15 | 52.36 | 142.91 |
| 418.15 | 55.79 | 151.15 |
| 423.15 | 59.51 | 160.00 |
| 428.15 | 63.50 | 169.36 |
| 431.15 | 66.00 | 175.19 |

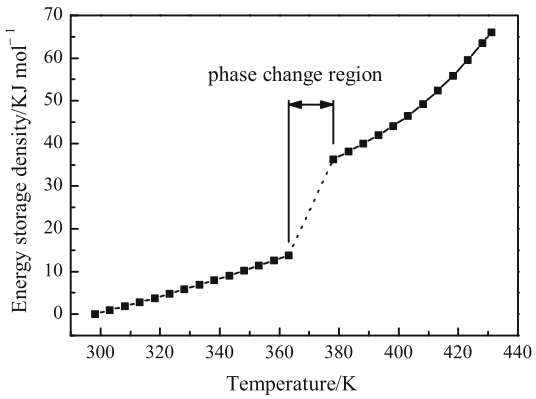


**Fig. 4** Energy storage curve of the PCM

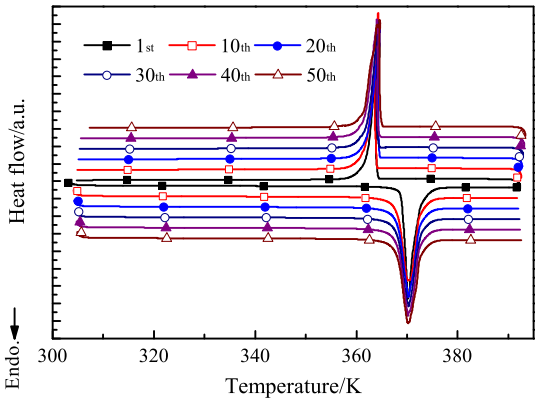


**Fig. 5** The 1st, 10th, 20th, 30th, 40th and 50th heating and cooling cyclic DSC curves of the PCM

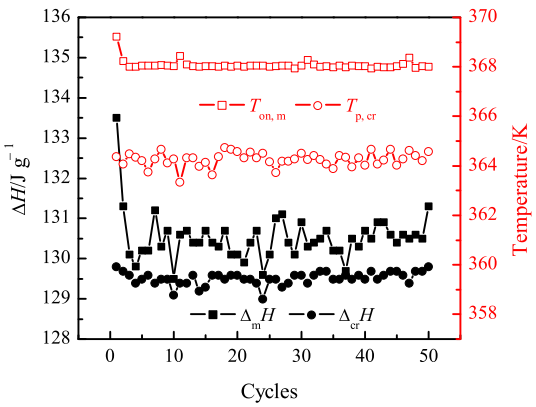


**Fig. 6** $\Delta_m H$, $\Delta_{cr} H$, $T_{on,m}$ and $T_{on,cr}$ of the PCM in 50 cyclic DSC experiment (mean values of three duplicated experiments with different samples; the uncertainties are ± 0.5 K for $T$ and ± 5% for $\Delta H$)

$T_{on,m}$ of the PCM was slightly decreased from 369 to 368 K after the first cycle and then stabilized at this temperature in the subsequent cycles, while the $T_{p,cr}$ of the PCM was stabilized at about 364 K over all the 50 cycles. It can be seen that the PCM exhibited slight supercooling when it crystallized from liquid. The degree of supercooling of the PCM should be smaller than the difference between the $T_{on,m}$ and $T_{p,cr}$ since $T_{on,cr}$ is generally higher than $T_{p,cr}$. Besides, the supercooling can be alleviated in real applications when the sample mass is increased from several milligrams to bulky volume [36]. Hence, this $T_{p,cr}$ indicated that the PCM is suitable to be applied in solar absorption cooling system. On the other hand, the $\Delta_m H$ of the PCM was also slightly decreased after the first cycle and then remained stable at about 130.5 J g$^{-1}$ in the subsequent cycles, while the $\Delta_{cr} H$ of the PCM was stabilized at about 129.5 J g$^{-1}$ over all the 50 cycles. The stable $\Delta_m H$ and $\Delta_{cr} H$ revealed that the PCM possessed very stable thermal energy storage and release capacity. The $\Delta_{trans} H$ and the $C_{p,\ m}$ of the PCM are lower than some PCMs candidates, such as 1-naphthol, sorbitol and xylitol, that melt over the temperature range of 363–373 K; however, these reported PCMs candidates are not stable, showing high supercooling, allotropic phase transition, incongruent melting or even absence of recrystallization [14]. Hence, the stable and suitable phase change temperature, and the stable thermal energy storage/release capacity, of the PCM implied that it is a great PCM for solar absorption cooling.

## Thermal stability and thermal conductivity

The TG curve of the PCM is depicted in Fig. 7. It can be seen that the PCM underwent a one-step mass loss procedure and all the mass was lost, corresponding to the evaporation of the PCM. The mass loss procedure of the PCM was started at about 438.15 K and terminated at approximately 558.15 K. The starting temperature of the mass loss of the PCM was approximately 70 K higher than its melting temperature, indicating that it possesses good thermal stability for it to be applied as PCM.

Three duplicate experiments were carried out to measure the thermal conductivity of the PCM. The mean value of

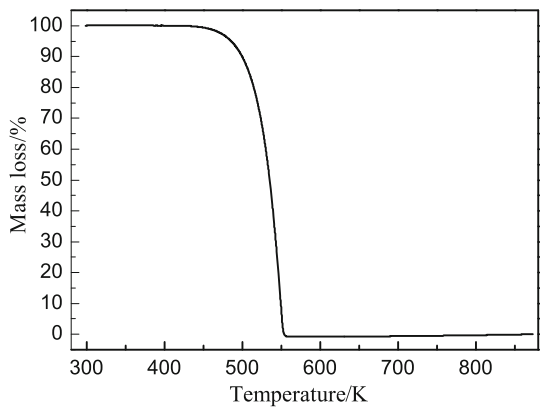


**Fig. 7** TG curve of the PCM

the three measurements was 0.197 W $m^{-1}$ $K^{-1}$ and the standard deviation was 0.003. The low thermal conductivity is normal for organic PCMs; however, it indicates that the thermal conductivity of the PCM needs to be improved for its application for thermal energy storage.

## Conclusions

We presented the thermal energy storage properties of a PCM candidate that could be applied in solar energy absorption cooling. The PCM melted and crystallized at 368 and 364 K, respectively, with the $\Delta_{trans}H$ of 21 kJ $mol^{-1}$ (130 J $g^{-1}$). A preliminary 50 cyclic DSC investigation shows that it possessed great long-term cyclic thermal energy storage stability. TG experiment revealed that the thermal stability of the PCM was satisfied for it to be applied as PCM. Hence, it could be applied as excellent PCM in solar energy absorption cooling. The thermal conductivity of the PCM was 0.197 W $m^{-1}$ $K^{-1}$, which indicates that the thermal conductivity of the PCM should be enhanced for its application for thermal energy storage. In addition, the heat capacities of the PCM were measured by means of TMDSC from 198.15 K to 431.15 K, and the thermodynamic functions of $[H_T–H_{298.15}]$ and $[S_T–S_{298.15}]$ were calculated based on the heat capacities data.

**Acknowledgements** This work was supported by the Natural Science Foundation of Hunan Province, China (2017JJ1026, 13JJ3068), the Scientific Research Fund of Hunan Provincial Education Department (15B0002) and the Guangxi Key Laboratory of Information Materials (Guilin University of Electronic Technology), P.R. China (171001-K).

## References

1. Balaras CA, Grossman G, Henning H-M, Infante Ferreira CA, Podesser E, Wang L, et al. Solar air conditioning in Europe—an overview. Renew Sustain Energy Rev. 2007;11(2):299–314. https://doi.org/10.1016/j.rser.2005.02.003.
2. Pintaldi S, Perfumo C, Sethuvenkatraman S, White S, Rosengarten G. A review of thermal energy storage technologies and control approaches for solar cooling. Renew Sustain Energy Rev. 2015;41:975–95. https://doi.org/10.1016/j.rser.2014.08.062.
3. Otanicar T, Taylor RA, Phelan PE. Prospects for solar cooling—an economic and environmental assessment. Sol Energy. 2012;86(5):1287–99. https://doi.org/10.1016/j.solener.2012.01.020.
4. Noro M, Lazzarin RM, Busato F. Solar cooling and heating plants: an energy and economic analysis of liquid sensible vs phase change material (PCM) heat storage. Int J Refrig. 2014;39:104–16. https://doi.org/10.1016/j.ijrefrig.2013.07.022.
5. Farid MM, Khudhair AM, Razack SAK, Al-Hallaj S. A review on phase change energy storage: materials and applications. Energy Convers Manag. 2004;45(9–10):1597–615.
6. Zeng JL, Zheng SH, Yu SB, Zhu FR, Gan J, Zhu L, et al. Preparation and thermal properties of palmitic acid/polyaniline/exfoliated graphite nanoplatelets form-stable phase change materials. Appl Energ. 2014;115:603–9. https://doi.org/10.1016/j.apenergy.2013.10.061.
7. Zeng J-L, Chen Y-H, Shu L, Yu L-P, Zhu L, Song L-B, et al. Preparation and thermal properties of exfoliated graphite/erythritol/mannitol eutectic composite as form-stable phase change material for thermal energy storage. Sol Energy Mater Sol Cells. 2018;178:84–90. https://doi.org/10.1016/j.solmat.2018.01.012.
8. Sami S, Etesami N. Thermal characterization of obtained microencapsulated paraffin under optimal conditions for thermal energy storage. J Therm Anal Calorim. 2017;130(3):1961–71. https://doi.org/10.1007/s10973-017-6516-9.
9. Hu Y, He Y, Zhang Z, Wen D. Effect of $Al_2O_3$ nanoparticle dispersion on the specific heat capacity of a eutectic binary nitrate salt for solar power applications. Energy Convers Manag. 2017;142:366–73. https://doi.org/10.1016/j.enconman.2017.03.062.
10. Agyenim F. The use of enhanced heat transfer phase change materials (PCM) to improve the coefficient of performance (COP) of solar powered LiBr/$H_2O$ absorption cooling systems. Renew Energy. 2016;87(Part 1):229–39. https://doi.org/10.1016/j.renene.2015.10.012.
11. Chidambaram LA, Ramana AS, Kamaraj G, Velraj R. Review of solar cooling methods and thermal storage options. Renew Sustain Energy Rev. 2011;15(6):3220–8. https://doi.org/10.1016/j.rser.2011.04.018.
12. Florides GA, Kalogirou SA, Tassou SA, Wrobel LC. Modelling, simulation and warming impact assessment of a domestic-size absorption solar cooling system. Appl Therm Eng. 2002;22(12):1313–25. https://doi.org/10.1016/S1359-4311(02)00054-6.
13. Vasilescu C, Infante Ferreira C. Solar driven double-effect absorption cycles for sub-zero temperatures. Int J Refrig. 2014;39(Supplement C):86–94. https://doi.org/10.1016/j.ijrefrig.2013.09.034.
14. Brancato V, Frazzica A, Sapienza A, Freni A. Identification and characterization of promising phase change materials for solar cooling applications. Sol Energy Mater Sol Cells. 2017;160(Supplement C):225–32. https://doi.org/10.1016/j.solmat.2016.10.026.
15. Khan MMA, Saidur R, Al-Sulaiman FA. A review for phase change materials (PCMs) in solar absorption refrigeration systems. Renew Sustain Energy Rev. 2017;76(Supplement C):105–37. https://doi.org/10.1016/j.rser.2017.03.070.
16. Zalba B, Marin JM, Cabeza LF, Mehling H. Review on thermal energy storage with phase change: materials, heat transfer analysis and applications. Appl Therm Eng. 2003;23(3):251–83.
17. Shkatulov A, Ryu J, Kato Y, Aristov Y. Composite material "Mg(OH)2/vermiculite": a promising new candidate for storage of middle temperature heat. Energy. 2012;44(1):1028–34. https://doi.org/10.1016/j.energy.2012.04.045.
18. Seo J, Shin D. Size effect of nanoparticle on specific heat in a ternary nitrate ($LiNO_3$–$NaNO_3$–$KNO_3$) salt eutectic for thermal energy storage. Appl Therm Eng. 2016;102:144–8. https://doi.org/10.1016/j.applthermaleng.2016.03.134.
19. Zhao CY, Ji Y, Xu Z. Investigation of the Ca(NO3)2–NaNO3 mixture for latent heat storage. Sol Energy Mater Sol Cells. 2015;140:281–8. https://doi.org/10.1016/j.solmat.2015.04.005.
20. Gunasekara SN, Pan R, Chiu JN, Martin V. Polyols as phase change materials for surplus thermal energy storage. Appl Energ. 2016;162:1439–52. https://doi.org/10.1016/j.apenergy.2015.03.064.
21. Zhang X, Chen X, Han Z, Xu W. Study on phase change interface for erythritol with nano-copper in spherical container during heat transport. Int J Heat Mass Transf. 2016;92:490–6. https://doi.org/10.1016/j.ijheatmasstransfer.2015.08.095.

22. Kholmanov I, Kim J, Ou E, Ruoff RS, Shi L. Continuous carbon nanotube–ultrathin graphite hybrid foams for increased thermal conductivity and suppressed subcooling in composite phase change materials. ACS Nano. 2015;9(12):11699–707. https://doi.org/10.1021/acsnano.5b02917.
23. Zeng JL, Zhou L, Zhang YF, Sun SL, Chen YH, Shu L, et al. Effects of some nucleating agents on the supercooling of erythritol to be applied as phase change material. J Therm Anal Calorim. 2017;129(3):1291–9. https://doi.org/10.1007/s10973-017-6296-2.
24. Lu DF, Di YY, Dou JM. Crystal structures and solid–solid phase transitions on phase change materials $(1-C_nH_{2n+1}NH_3)_2$-$CuCl_4$(s) ($n$ = 10 and 11). Sol Energy Mater Sol Cells. 2013;114:1–8. https://doi.org/10.1016/j.solmat.2013.02.009.
25. Emam M, Ahmed M. Cooling concentrator photovoltaic systems using various configurations of phase-change material heat sinks. Energy Convers Manag. 2018;158:298–314. https://doi.org/10.1016/j.enconman.2017.12.077.
26. Rivière L, Caussé N, Lonjon A, Dantras É, Lacabanne C. Specific heat capacity and thermal conductivity of PEEK/Ag nanoparticles composites determined by modulated-temperature differential scanning calorimetry. Polym Degrad Stab. 2016;127:98–104. https://doi.org/10.1016/j.polymdegradstab.2015.11.015.
27. Qiu S, Chu H, Zou Y, Xiang C, Zhang H, Sun L, et al. Thermochemical studies of Rhodamine B and Rhodamine 6G by modulated differential scanning calorimetry and thermogravimetric analysis. J Therm Anal Calorim. 2015;123(2):1611–8. https://doi.org/10.1007/s10973-015-5055-5.
28. Zhang J, Liu YY, Zeng JL, Xu F, Sun LX, You WS, et al. Thermodynamic properties and thermal stability of the synthetic zinc formate dihydrate. J Therm Anal Calorim. 2008;91(3):861–6. https://doi.org/10.1007/s10973-007-8587-5.
29. Chen C, Liu W, Wang Z, Peng K, Pan W, Xie Q. Novel form stable phase change materials based on the composites of polyethylene glycol/polymeric solid-solid phase change material. Sol Energy Mater Sol Cells. 2015;134:80–8. https://doi.org/10.1016/j.solmat.2014.11.039.
30. Yanshan L, Shujun W, Hongyan L, Fanbin M, Huanqing M, Wangang Z. Preparation and characterization of melamine/formaldehyde/polyethylene glycol crosslinking copolymers as solid–solid phase change materials. Sol Energy Mater Sol Cells. 2014;127:92–7. https://doi.org/10.1016/j.solmat.2014.04.013.
31. Li R-C, Tan Z-C. Heat capacity and thermodynamic property studies of diethyl acetamidomalonate (C9H15NO5). J Chem Eng Data. 2013;58(8):2137–41. https://doi.org/10.1021/je400159e.
32. Chirico RD, Steele WV, Kazakov AF. Thermodynamic properties of 1-naphthol: mutual validation of experimental and computational results. J Chem Thermodyn. 2015;86:106–15. https://doi.org/10.1016/j.jct.2015.02.008.
33. Tong B, Tan ZC, Shi Q, Li YS, Wang SX. Thermodynamic investigation of several natural polyols (II). J Therm Anal Calorim. 2008;91(2):463–9. https://doi.org/10.1007/s10973-007-8361-8.
34. Jia R, Sun K, Li R, Zhang Y, Wang W, Yin H, et al. Heat capacities of some sugar alcohols as phase change materials for thermal energy storage applications. J Chem Thermodyn. 2017;115:233–48. https://doi.org/10.1016/j.jct.2017.08.004.
35. Zhang XF, Wang SF, Wu ZS. Physical chemistry. Wuhan: Huazhong University of Science & Technology Press; 2012.
36. Adachi T, Daudah D, Tanaka G. Effects of supercooling degree and specimen size on supercooling duration of erythritol. ISIJ Int. 2014;54(12):2790–5. https://doi.org/10.2355/isijinternational.54.2790.